The $\alpha_3(\beta Met^{222}Ser/Tyr^{345}Trp)_3\gamma$ Subcomplex of the TF_1-ATPase Does Not Hydolyze ATP at a Significant Rate until the Substrate Binds to the Catalytic Site of the Lowest Affinity†

Huimiao Ren,‡ Sanjay Bandyopadhyay,§ and William S. Allison*,‖

Applied Biotech, Inc., 10237 Flanders Court, San Diego, California 92121, Department of Biotechnology, Zydus Research Center, Ahmedabad 3802213, Gujarat, India, and Department of Chemistry and Biochemistry, University of California—San Diego, La Jolla, California 92093-0601

Received February 3, 2006; Revised Manuscript Received March 21, 2006

ABSTRACT: The $\alpha_3(\beta M^{222}S/Y^{345}W)_3\gamma$ double-mutant subcomplex of the F_1-ATPase from the thermophilic *Bacillus* PS3 (TF_1), free of endogenous nucleotides, does not entrap inhibitory MgADP in a catalytic site during turnover. It hydrolyzes 100 nM−2 mM ATP with a K_m of 31 μM and a k_{cat} of 220 s^{-1}. Fluorescence titrations of the introduced tryptophans with MgADP or MgATP revealed that both Mg−nucleotide complexes bind to the catalytic site of the highest affinity with K_{d_1} values of less than 1 nM and bind to the site of intermediate affinity with a common K_{d_2} value of about 12 nM. The K_{d_3} values obtained for the catalytic site of the lowest affinity from titrations with MgADP and MgATP are 25 and 37 μM, respectively. The double mutant hydrolyzes 200 nM ATP with a first-order rate of 1.5 s^{-1}, which is 0.7% of k_{cat}. Hence, it does not hydrolyze ATP at a significant rate when the catalytic site of intermediate affinity is saturated and the catalytic site of the lowest affinity is minimally occupied. After the addition of stoichiometric MgATP to the $\alpha_3(\beta M^{222}S/Y^{345}W)_3\gamma$ subcomplex, one-third of the tryptophan fluorescence remains quenched after 10 min. The product [^{3}H]ADP remains bound when the wild-type and double-mutant subcomplexes hydrolyze substoichiometric [^{3}H]ATP. In contrast, $^{32}P_i$ is not retained when the wild-type subcomplex hydrolyzes substoichiometric [γ-^{32}P]ATP. This precludes assessment of the equilibrium at the high-affinity catalytic site when the wild-type TF_1 subcomplex hydrolyzes substoichiometric ATP.

The F_1-ATPase is the peripheral membrane component of the F_oF_1-ATP synthases that couple proton electrochemical gradients to ATP synthesis in energy-transducing membranes (*1*). When removed from F_o as an $\alpha_3\beta_3\gamma\delta\epsilon$ oligomer, F_1 catalyzes ATP hydrolysis. In crystal structures of F_1-ATPase from bovine heart mitochondria (MF_1)[1] (*2*−*5*), the α and β subunits are elongated and arranged alternately in an $(\alpha\beta)_3$ hexamer. The central cavity of the $(\alpha\beta)_3$ hexamer is occupied by an asymmetric coiled coil consisting of the α-helical amino and carboxyl termini of the γ subunit.

F_1 contains six nucleotide-binding sites, three of which are catalytic sites that are located mostly on β subunits at α/β interfaces. The other three, called noncatalytic sites, do not have a well-defined physiological role. Noncatalytic sites are located mostly on α subunits at interfaces of α/β pairs that differ from those that comprise catalytic sites. Noncatalytic sites are occupied with either Mg 5′-adenylyl-β,γ-imidophosphate (AMP−PNP) (*2*, *3*) or MgADP (*4*, *5*) in different crystal structures of bovine MF_1. In the original crystal structure, the three β subunits are heterogeneously liganded (*2*). One, designated β_{TP}, contains MgAMP−PNP; another, designated β_{DP}, contains MgADP; and the third, designated β_E, is empty. The conformations of β_{TP} and β_{DP} are very similar to each other. In contrast, β_E has a considerably different, open conformation. The α subunits that contribute to catalytic sites of β_{TP}, β_{DP}, and β_E are designated α_{TP}, α_{DP}, and α_E, respectively.

Entrapment of inhibitory MgADP in a catalytic site during turnover complicates determination of the characteristics of steady-state ATP hydrolysis catalyzed by F_1-ATPase (*6*). Lineweaver−Burk plots constructed from rates of ATP hydrolysis catalyzed by MF_1 and the wild-type $\alpha_3\beta_3\gamma$ subcomplex of the F_1-ATPase from the thermophilic *Bacillus* PS3 (TF_1) are biphasic in the absence of activators that overcome turnover-induced entrapment of inhibitory MgADP. Entrapment of inhibitory MgADP is provoked by azide anion, which appears to stabilize the inhibitory complex. Entrapment of inhibitory MgADP during ATP hydrolysis catalyzed by MF_1 is relieved by including pyrophosphate in

† This work was supported by NIGMS Grant GM 16974 from the National Institutes of Health.

* To whom correspondence should be addressed: Department of Chemistry and Biochemistry, University of California−San Diego, La Jolla, CA 92093-0601. Telephone: 858-534-3057. Fax: 858-534-7390. E-mail: wsa@checfs2.ucsd.edu.

‡ Applied Biotech, Inc.

§ Zydus Research Center.

‖ University of California−San Diego.

[1] Abbreviations: MF_1, TF_1, and EF_1, the F_1-ATPases from bovine heart mitochondria, the thermophilic *Bacillus* PS3, and *Escherichia coli*, respectively; ANP, ADP plus ATP; AMP−PNP, 5′-adenylyl-β,γ-imidophosphate; CDTA, *trans*-1,2-diaminocyclohexane-*N*,*N*,*N*′,*N*′-tetra-acetic acid; LDAO, lauryldimethylamine oxide; DCCD, *N*,*N*′-dicyclohexylcarbodiimide; $ndMF_1$, bovine MF_1 depleted of endogenous nucleotides; Mg-PP_i, magnesium pyrophosphate.

10.1021/bi060232w CCC: $33.50
Published on Web 04/25/2006

the assay medium (*7*). In the case of the $\alpha_3\beta_3\gamma$ subcomplex of TF_1, entrapment of inhibitory MgADP is relieved by including the nonionic detergent lauryldimethylamine oxide (LDAO) in the assay medium (*8*). Pyrophosphate does not affect entrapment of inhibitory MgADP during ATP hydrolysis by TF_1 or its $\alpha_3\beta_3\gamma$ subcomplex.

Single-molecule experiments, designed on the basis of the original crystal structure of MF_1, have shown that the $\alpha_3\beta_3\gamma$ subcomplex of TF_1 is a rotary motor that couples sequential hydrolysis of ATP at the three catalytic sites of the enzyme to rotation of the γ subunit in discrete 120° steps (*9*). Moreover, imaging in the submillisecond time range showed that each 120° rotational step occurs in 30° and 90° substeps (*10*). Because the length of the pause preceding the 90° substep depends upon the ATP concentration, ATP binding initiates this substep. The pause preceding the 30° substep is thought to represent the time required to release products from an alternate catalytic site to reset the system for another round of catalysis.

Whether ATP hydrolysis by F_1-ATPases under conventional conditions occurs with a bi- or trisite mechanism is controversial. According to the bisite model introduced by Boyer in the 1970s, saturation of two catalytic sites is sufficient to attain maximal rates of ATP hydrolysis (*11*). The bisite activation model gained considerable support when it was reported that the bovine mitochondrial and *Escherichia coli* F_1-ATPases hydrolyze substoichiometric [γ-^{32}P]ATP at a high-affinity catalytic site slowly with an apparent equilibrium constant of about 1 (*12*, *13*). After hydrolysis of substoichiometric [γ-^{32}P]ATP, the addition of millimolar concentrations of MgATP to the preloaded enzymes promoted the rapid release of [^{32}P]P_i, indicating that binding of the substrate to a second catalytic site of lower affinity drives complete ATP hydrolysis and release of products from the initially loaded high-affinity catalytic site.

General acceptance of the bisite activation model diminished after Weber et al. (*14*) correlated the affinities of catalytic sites for MgATP, assessed from nucleotide-induced fluorescence quenching of the introduced tryptophans in the $\beta Y^{345}W$ mutant[2] of the F_1-ATPase from *E. coli* (EF_1), with the concentration of ATP required to observe significant rates of ATP hydrolysis. The mutant enzyme, which exhibited three K_d values for MgATP, did not attain maximal velocity until the third catalytic site, that of the lowest affinity for MgATP, was saturated.

In defense of the bisite activation model, Boyer and colleagues (*15*) have argued that fluorescence titrations of the $\beta Y^{345}W$ mutant of EF_1 could be adversely affected by the dissociation of the ϵ subunit during fluorescence titrations and/or entrapment of inhibitory MgADP in a catalytic site during titrations with MgATP. In support of the second reservation, it is clear that entrapment of inhibitory MgADP prevents determination of a distinct K_{d_2} value from fluorescence titrations of the introduced tryptophans in catalytic sites, the $\alpha_3(\beta Y^{345}W)_3\gamma$ single-mutant and $\alpha_3(\beta E^{199}V/Y^{345}W)_3\gamma$ double-mutant subcomplexes of TF_1 (*16*−*18*).

This controversy arose again recently when Milgrom and Cross (*19*) reported that bovine MF_1, nearly free of endogenous nucleotides, attains maximal velocity of ATP hydrolysis when two of the three catalytic sites are saturated with MgATP. In conflict with their conclusion based on analysis of MF_1, we report here that the $\alpha_3(\beta M^{222}S/Y^{345}W)_3\gamma$ double-mutant subcomplex of TF_1, free of endogenous nucleotides, does not entrap inhibitory MgADP in a catalytic site during turnover and does not hydrolyze ATP at a significant rate until the catalytic site of the lowest affinity binds MgATP.

EXPERIMENTAL PROCEDURES

Materials. Enzymes and biochemicals used in assays and buffers were purchased from Sigma. Primers for mutations were purchased from Gibco Life Technologies. LDAO was purchased from Calbiochem. Both [2,8-^{3}H]ATP and [γ-^{32}P]ATP were purchased from NEN Life Science Products. Liquid scintillation counting was performed with Ecoscint obtained from National Diagnostics.

Generation of Mutant Subcomplexes. Plasmid pKK, which carries the genes for the α, β, and γ subunits of TF_1, was used for mutagenesis and gene expression (*20*). Mutant expression plasmids were prepared by the polymerase chain reaction using the QuikChange mutagenesis kit from Stratagene. The $\beta M^{222}S$ and $\beta Y^{345}W$ substitutions were introduced separately by PCR into the pTD plasmid carrying the genes encoding the α, β, and γ subunits of TF_1 as a template. To prepare the $\alpha_3(\beta M^{222}S/Y^{345}W)_3\gamma$ double mutant, the $\beta Y^{345}W$ substitution was introduced with PCR into pTD($\beta M^{222}S$) as a template. The primers used for mutagenesis were 5′-GTCTTCGGACAAAGCAATGAGCCGCCG-3′ and 5′-CGGCGGCTCATTGCTTTGTCCGAACAC-3′ for the $\beta M^{222}S$ substitution and 5′-GCGGAGATGGGGATTTGGC-CGGCCGTTGACCC-3′ and 5′-GGGTCAACGGCCGGCC-AAATCCCCATCTCCGC-3′ for the $\beta Y^{345}W$ substitution. Changed bases are underlined. The mutations were confirmed by sequencing. The *Pst* I−*Mlu* I fragment containing the gene encoding β subunit from the resultant pTD plasmid was ligated into the *Pst* I−*Mlu* I site of pKK to produce the expression plasmid pKK-$\beta M^{222}S/Y^{345}W$. Purification of the wild-type and mutant subcomplexes was performed as described by Matsui and Yoshida (*20*). Wild-type and mutant subcomplexes were stored at 4 °C as precipitates in 70% saturated ammonium sulfate.

Analytical Methods. Enzyme stock solutions were prepared by dissolving pelleted ammonium sulfate precipitates, obtained by centrifugation, in 50 mM Tris-Cl at pH 8.0 containing 10 mM *trans*-1,2-diaminocyclohexane-*N*,*N*,*N*′,*N*′-tetraacetic acid (CDTA). After 1 h at room temperature, the dissolved enzymes were passed through a 1 mL centrifuge column of Sephadex G-50 (*21*) equilibrated with 50 mM Tris-Cl at pH 8.0 containing 0.1 mM ethylenediaminetetraacetic acid (EDTA). After this treatment, the enzyme subcomplexes were essentially free of bound nucleotides as assessed by anion-exchange high-performance liquid chromatography (HPLC) as described previously (*17*). Protein concentrations were determined by the method of Bradford (*22*) using Coomassie Blue (Pierce).

ATPase activity was determined spectrophotometrically with an ATP regeneration system at 30 °C and pH 8.0. Assays were performed with a Kontron Instruments Uvikon-933 double-beam spectrophotometer attached to a chart

[2] Unless stated otherwise, residue numbers of MF_1 are used throughout. In MF_1, βE^{188}, βM^{222}, βR^{260}, and βY^{345} are equivalent, respectively, to βE^{199}, βM^{218}, βR^{256}, and βY^{341} in TF_1 and βE^{181}, βM^{209}, βR^{246}, and βY^{331} in EF_1.

recorder. In most cases, recorded traces of decreasing absorption at 340 nm were initiated within 3 s after injecting enzyme solutions into rapidly stirred assay medium containing various concentrations of ATP, 200 μM NADH, 30 mM KCl, 4 mM phosphoenolpyruvate, 20 μg/mL lactate dehydrogenase, 40 μg/mL pyruvate kinase, and $MgCl_2$ in 50 mM Tris-Cl at pH 8.0. Unless indicated otherwise, the $MgCl_2$ concentration was 1 mM in excess of the ATP concentration. When assays were initiated with Mg^{2+} ion, 10 μL of 100 mM $MgCl_2$ was injected into 1 mL of rapidly of stirred assay medium containing 1 μg of the wild-type or $\beta M^{222}S/Y^{345}W$ subcomplex, 50 μM ATP, 200 μM NADH, 30 mM KCl, 4 mM phosphoenolpyruvate, 20 μg/mL lactate dehydrogenase, and 40 μg/mL pyruvate kinase in 50 mM Tris-Cl at pH 8.0.

Fluorescence titrations of the introduced tryptophans in the $\beta M^{222}S/Y^{345}W$ double mutant with nucleotides were performed by injecting small volumes of nucleotides at high concentrations into 3.0 mL of rapidly stirred 50 nM mutant enzyme in 50 mM Tris-Cl at pH 8.0 contained in a cuvette mounted in a Spex Fluoromax-2 spectrofluorometer. Fluorescence measurements were recorded 30 s after the addition of the nucleotide. The excitation and emission wavelengths were 295 and 355 nm, respectively. In titrations with MgADP or MgATP, $MgCl_2$ was present in 1 mM excess over the concentration of ADP or ATP. The buffer used in titrations with ATP in the absence of $MgCl_2$ contained 0.1 mM EDTA. Fresh enzyme solutions were prepared for each concentration of MgATP examined. The free nucleotide concentrations shown in Figure 5 were established by subtracting the amount of bound nucleotide, determined from fluorescence quenching, from the total amount of nucleotide added. K_d values were calculated by nonlinear regression analysis using SigmaPlot with the equation described by Weber et al. (*14*).

Hydrolysis of ATP at a Single Catalytic Site. Hydrolysis of substoichiometric ATP was initiated by rapidly mixing 2.85 μM (1 mg/mL) wild-type subcomplex with 1.7 μM [^{3}H]ATP or [γ-^{32}P]ATP in the presence of 1 mM $MgCl_2$ in 50 mM Tris-Cl at pH 8.0. Rates of hydrolysis of the substoichiometric [^{3}H]ATP and [γ-^{32}P]ATP were determined by withdrawing 75 μL samples of the reaction mixture at several time intervals and mixing them with 2 μL of 60% perchloric acid in 0.5 mL centrifuge tubes. After 10 min, perchloric acid was neutralized by the addition of 2 μL of 9.2 M KOH. After neutralization, the samples were placed in an ice bath for 10 min. Precipitated $KClO_4$ and denatured enzyme were then removed by centrifugation. The extent of hydrolysis of the [^{3}H]ATP or [γ-^{32}P]ATP was determined by submitting samples of the supernatants to anion-exchange HPLC as described previously (*17*). The quantities of [^{3}H]ADP or $^{32}P_i$ in the effluents were determined by liquid scintillation counting. The amount of [^{3}H]ADP remaining bound to the wild-type enzyme during hydrolysis of [^{3}H]ATP was determined by passing 75 μL samples of the reaction mixture, at increasing time intervals, through 1 mL centrifuge columns of Sephadex G-50, equilibrated with 50 mM Tris-Cl, into test tubes containing 2 μL of 60% perchloric acid. The amount of $^{32}P_i$ remaining bound to the wild-type enzyme after hydrolysis of [γ-^{32}P]ATP was determined by the same method.

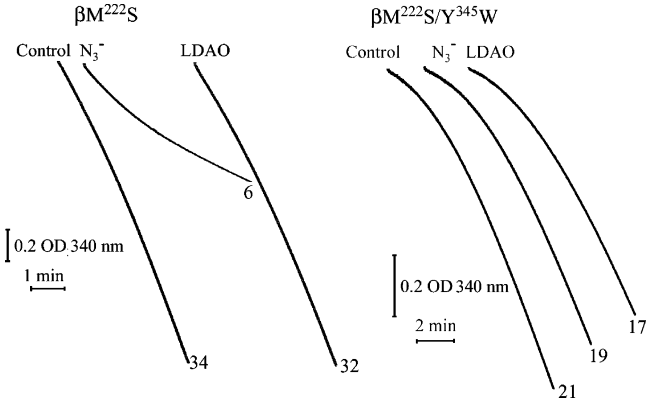

FIGURE 1: Effects of azide and LDAO on the hydrolysis of 50 μM ATP by the $\beta M^{222}S$ and $\beta M^{222}S/Y^{345}W$ mutant subcomplexes. Solutions of the subcomplexes at 1 mg/mL in 50 mM Tris-Cl at pH 8.0 containing 0.1 mM EDTA were prepared as described in the Experimental Procedures. Rates of ATP hydrolysis were recorded within 3 s after injecting 1 μg of the $\beta M^{222}S$ single mutant or 1 μg of the $\beta M^{222}S/Y^{345}W$ double mutant into the assay medium containing 50 μM ATP and the following additions: (control), no additions; (N_3^-), 1 mM NaN_3; or (LDAO), 0.06% LDAO.

RESULTS

The $\alpha_3(\beta M^{222}S/Y^{345}W)_3\gamma$ Double Mutant Hydrolyzes 50 μM ATP with a Linear Rate after Incubation with ATP or MgADP prior to Initiating Assays. As shown earlier (*16*) and in Figures 2 and 3B, the wild-type $\alpha_3\beta_3\gamma$ subcomplex of TF_1 hydrolyzes ATP in three phases when it is injected into an ATP regeneration system containing 50 μM ATP. An initial burst of ATP hydrolysis rapidly declines to a slower, intermediate rate that gradually accelerates to a final rate of about 8 μmol of ATP hydrolyzed mg^{-1} min^{-1}. In the presence of 1 mM NaN_3, wild-type enzyme hydrolyzes 50 μM ATP with a burst that rapidly declines to a very slow rate. In contrast, in the presence of 0.06% LDAO, it hydrolyzes 50 μM ATP with a linear initial rate that is about 3-fold greater than the final rate observed in the absence of LDAO. It was also shown previously that, in the absence of LDAO and azide, the $\beta Y^{345}W$ mutant hydrolyzes 50 μM ATP with a barely detectable initial burst that slowly accelerates to a final rate of about 7 μmol of ATP hydrolyzed mg^{-1} min^{-1}. Hydrolysis of 50 μM ATP by the $\beta Y^{345}W$ mutant is less sensitive to inhibition by 1 mM NaN_3 than the wild-type enzyme and is only slightly stimulated by 0.06% LDAO (*18*).

Figure 1 compares the rates of hydrolysis of 50 μM ATP by the $\beta M^{222}S$ single-mutant and $\beta M^{222}S/Y^{345}W$ double-mutant subcomplexes under three conditions: (a) in the absence of additions, (b) in the presence of 1 mM NaN_3, and (c) in the presence of 0.06% LDAO. The traces of NADH consumption shown in Figure 1 were recorded from less than 3 s to several minutes after injecting the mutant enzymes into an ATP-regenerating system containing 50 μM ATP. The numbers at the ends of the traces represent rates of ATP hydrolysis recorded over the last 1 min of the assay expressed in μmol of ATP hydrolyzed mg^{-1} min^{-1}. In the absence of additions, the $\beta M^{222}S$ mutant hydrolyzes 50 μM ATP with a slightly accelerating rate in the absence of an initial burst. The final rate is about 5-fold greater than the final rate observed with the wild-type enzyme. In comparison with the wild-type enzyme, the single-mutant enzyme is less

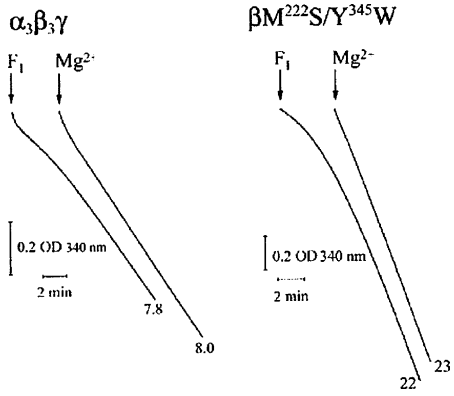

FIGURE 2: Comparison of rates of hydrolysis of 50 μM ATP by the wild-type and $\beta M^{222}S/Y^{345}W$ double-mutant subcomplexes when assays were initiated with enzyme or $MgCl_2$. The wild-type and double-mutant subcomplexes at 1 mg/mL in 50 mM Tris-Cl at pH 8.0 containing 0.1 mM EDTA were prepared as described in the Experimental Procedures. In assays initiated with F_1, 1 μg of the wild-type or double-mutant enzyme was injected into the ATP regeneration system described in the Experimental Procedures containing 50 μM ATP and 1.05 mM $MgCl_2$. Assays initiated by injecting Mg^{2+} ion into the assay medium are described in the Experimental Procedures. Recordings of initial rates were initiated within 3 s after the injections.

sensitive to inhibition by 1 mM NaN_3 and is slightly inhibited, rather than stimulated by 0.06% LDAO. In contrast, the $\beta M^{222}S/Y^{345}W$ double mutant hydrolyzes 50 μM ATP in the presence or absence of either 1 mM NaN_3 or 0.06% LDAO with a sluggish initial rate that slowly accelerates to a final rate, which is about 3-fold greater than the final rate observed with the wild-type enzyme. Unlike the responses of the wild-type and $\beta M^{222}S$ and $\beta Y^{345}W$ single-mutant enzymes to azide and LDAO, hydrolysis of 50 μM ATP by the double-mutant enzyme is only slightly inhibited by 1 mM NaN_3 and is slightly inhibited, rather than stimulated, by 0.06% LDAO.

Figure 2 compares the rates of hydrolysis of 50 μM ATP by the wild-type and $\beta M^{222}S/Y^{345}W$ double-mutant enzymes when assays were initiated by (a) injecting the enzyme into the ATP regeneration system containing 50 μM ATP plus 1.05 mM $MgCl_2$ or (b) injecting $MgCl_2$, to a final concentration of 1.05 mM, into the assay medium containing the enzyme and 50 μM ATP in the absence of $MgCl_2$. When the $\beta M^{222}S/Y^{345}W$ double mutant was incubated with 50 μM ATP in the assay medium free of $MgCl_2$ for 10 min before injecting $MgCl_2$ to initiate ATP hydrolysis, a linear rate was observed within 3 s of the injection. In contrast, Figure 2 also shows that a fast rate rapidly declined to a slower rate when the wild-type enzyme was assayed under the same conditions. It is important to note that, in experiments not illustrated, nonlinear, accelerating initial rates were observed when assays were initiated by injecting $MgCl_2$ into the ATP-regenerating system containing the double-mutant enzyme and less than 30 μM ATP.

Figure 3A shows the rates of hydrolysis recorded within 3 s of injecting 1 μg of the $\beta M^{222}S/Y^{345}W$ double-mutant enzyme, which had been incubated at 1.43 μM with increasing concentrations of MgADP for 30 min, into an ATP regeneration system containing 50 μM ATP and 1.05 mM $MgCl_2$. Linear rates of ATP hydrolysis were observed after incubating the double-mutant enzyme with 10 μM or greater MgADP but not with 5 μM or lower MgADP before

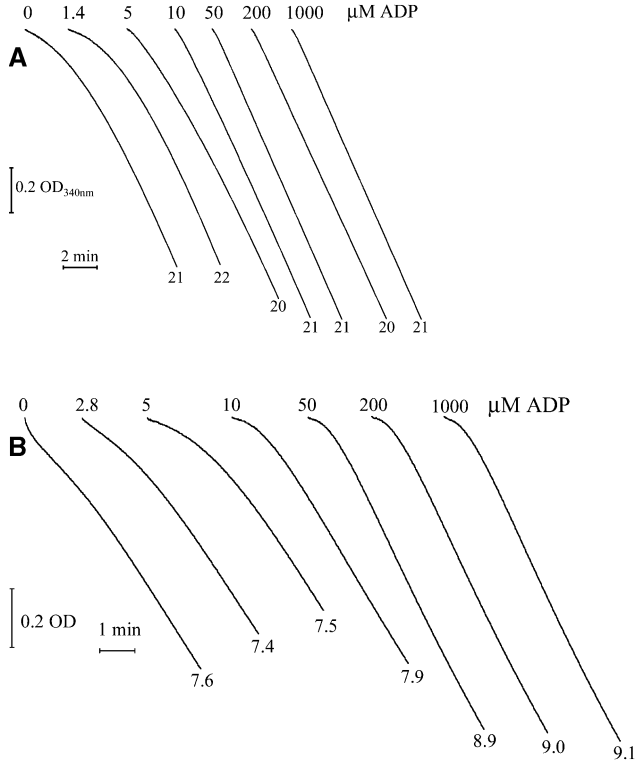

FIGURE 3: Comparison of the effects of prior incubation of the $\beta M^{222}S/Y^{345}W$ double-mutant and wild-type enzymes with increasing MgADP concentrations on rates of hydrolysis of 50 μM ATP. Rates of ATP hydrolysis were recorded within 3 s after injecting the double-mutant (A) or wild-type (B) enzyme, treated with various concentrations of MgADP, into a regeneration system containing 50 μM ATP. (A) $\beta M^{222}S/Y^{345}W$ double mutant at 0.5 mg/mL was incubated with 1 mM $MgCl_2$ in excess of the indicated ADP concentrations in 50 mM Tris-Cl at pH 8.0 for 30 min before assaying 1 μg samples of the treated enzyme with the ATP regeneration system described in the Experimental Procedures containing 50 μM ATP and 1 mM $MgCl_2$. (B) Traces illustrated for the wild-type subcomplex were obtained in the same manner except that they was incubated at 1.0 mg/mL with the concentrations of MgADP indicated for 30 min before initiating assays with 2 μg of enzyme.

Table 1: Comparison of the Effects of 1 mM NaN_3 and 0.06% LDAO on the Rates of Hydrolysis of 2 mM ATP by the Wild-Type and Mutant Subcomplexes

enzyme	percent of inhibition by 1 mM NaN_3 (%)	effects of 0.06% LDAO
$\alpha_3\beta_3\gamma$	96	4-fold activation
$\alpha_3(\beta Y^{345}W)_3\gamma$	73	1.95-fold activation
$\alpha_3(\beta M^{222}S)_3\gamma$	67	no effect
$\alpha_3(\beta M^{222}S/Y^{345}W)_3\gamma$	9	10% inhibition

initiating assays. Figure 3B shows that rapid, linear rates were not observed after incubating 2.8 μM wild-type enzyme with MgADP concentrations up to 1 mM under the same conditions prior to initiating assays.

Comparison of the Effects of NaN_3 and LDAO on Hydrolysis of 2 mM ATP by the Wild-Type and Mutant Subcomplexes. Table 1 compares the effects of 1 mM NaN_3 and 0.06% LDAO on the rates of hydrolysis of 2 mM ATP by the wild-type and mutant subcomplexes. Each mutant enzyme is less sensitive to inhibition by azide than the wild-type subcomplex. Whereas hydrolysis of 2 mM ATP by the $\beta M^{222}S$ and $\beta Y^{345}W$ single-mutant enzymes was inhibited by 67 and 73%, respectively, in the presence of 1 mM NaN_3,

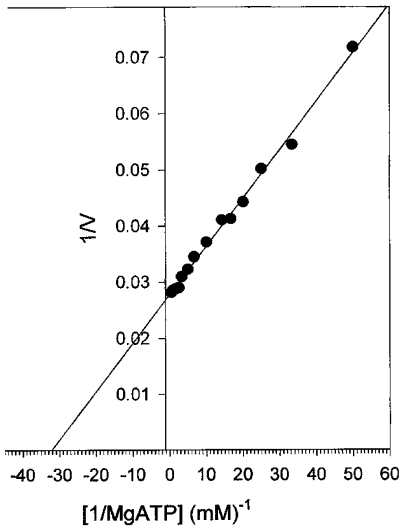

FIGURE 4: Lineweaver−Burk plot for the $\beta M^{222}S/Y^{345}W$ mutant enzyme obtained from linear rates of hydrolysis of 20 μM−2 mM ATP recorded from 8 to 9 min after iniating ATP hydrolysis. The double-mutant enzyme at 0.25 mg/mL was incubated with 200 μM MgADP for 30 min before injecting 2 μL samples into an ATP-regenerating system described in the Experimental Procedures containing 20−2000 μM ATP and 1 mM $MgCl_2$ in excess of the ATP concentration.

the $\beta M^{222}S/Y^{345}W$ double mutant was inhibited by only 9% under these conditions. Therefore, it has a very low propensity to entrap inhibitory MgADP in a catalytic site during turnover. This contention is supported by the observation that 0.06% LDAO slightly inhibits, rather than stimulates, hydrolysis of 2 mM ATP by the double-mutant enzyme.

Steady-State Kinetic Analysis of the $\beta M^{222}S/Y^{345}W$ Double-Mutant Subcomplex. The preliminary experiments illustrated in Figures 2 and 3 were performed to find a method for determining the K_m and V_{max} values of the $\beta M^{222}S/Y^{345}W$ double-mutant enzyme. In experiments not illustrated, a linear Lineweaver−Burk plot was obtained from initial rates that were recorded for hydrolysis of 20−2000 μM by 1 μg of the $\beta M^{222}S/Y^{345}W$ double mutant after the enzyme was incubated at 0.5 mg/mL with 200 μM MgADP for 30 min. The K_m and V_{max} values obtained from the linear plot were 32 μM and 34 μmol of ATP hydrolyzed mg^{-1} min^{-1}, respectively. Owing to the 200 μM MgADP present in the buffer during prior incubation, this method was not appropriate for determining rates of hydrolysis of significantly lower concentrations of ATP.

Figures 1 and 2 show that the slow, initial rates observed when the $\beta M^{222}S/Y^{345}W$ mutant was injected into the assay medium containing 50 μM ATP became linear after about 5 min. From this observation, the Lineweaver−Burk plot shown in Figure 4 was constructed from the linear rates of ATP hydrolysis recorded between 8 and 9 min after injecting 0.25 μg of the double-mutant enzyme into an ATP regeneration system containing 20−2000 μM ATP. The K_m and V_{max} values obtained from the plot are 31 μM and 37 μmol of ATP hydrolyzed mg^{-1} min^{-1}, respectively.

Given that commercial preparations of NADH contain small amounts of ADP, the following method was used to determine rates of hydrolysis of 100−400 nM ATP. Traces

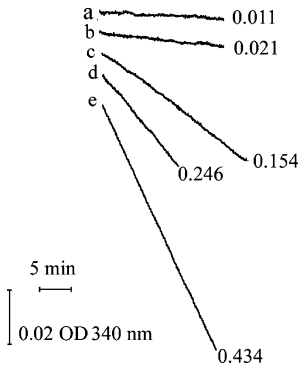

FIGURE 5: Rates of hydrolysis of 100−400 nM ATP by the $\beta M^{222}S/Y^{345}W$ double-mutant subcomplex. The recorded traces were initiated 5 min after injecting 1 μg of the $\beta M^{222}S/Y^{345}W$ double-mutant subcomplex into 0.8 mL of the ATP regeneration system described in the Experimental Procedures containing 1 mM $MgCl_2$ with the following modifications. Traces a and b are the rates of consumption of 10 μM NADH and 20 μM NADH, respectively, in the absence of added ATP. Traces c and d are the rates of consumption of 10 μM NADH in the regeneration system in the presence of 100 and 200 nM ATP, respectively. Trace e represents the rate of consumption of 20 μM NADH in the regeneration system in the presence of 400 nM ATP. The numbers at the end of the traces represent the rates of ATP hydrolysis expressed in μmol (mg of enzyme)$^{-1}$ min^{-1}.

Table 2: Comparison of the Calculated and Experimental Rates of Hydrolysis of 100−400 nM MgATP by the $\alpha_3(\beta M^{222}S/Y^{345}W)_3\gamma$ Subcomplex

ATP concentration (nM)	100	200	400
calculated rate (μmol of ATP min^{-1} mg^{-1})[a]	0.119	0.237	0.471
experimental rate (μmol of ATP min^{-1} mg^{-1})[b]	0.143	0.235	0.413

[a] Calculated with a V_{max} of 37 μmol of ATP hydrolyzed mg^{-1} min^{-1} and a K_m of 31 μM, values obtained from Figure 4. [b] Corrected for the rate observed with 10 μM NADH alone (100 and 200 nM ATP) and the rate observed with 20 μM NADH alone (400 nM ATP).

a and b in Figure 5 illustrate rates of NADH consumption observed after injecting 1 μg of the nucleotide-free $\beta M^{222}S/Y^{345}W$ mutant enzyme into an ATP regeneration system containing 10 and 20 μM NADH, respectively, in the absence of added ATP. The numbers at the end of traces, which were initiated 5 min after the addition of the enzyme, are the rates of NADH consumption, expressed in μmol oxidized min^{-1} (mg of enzyme)$^{-1}$, that were recorded between 10 and 15 min after the addition of the enzyme. The observed rate doubled when the NADH concentration in the assay medium was increased from 10 to 20 μM, confirming that the NADH used in these experiments contained contaminating ADP. Traces c and d in Figure 5 were obtained after injecting the double-mutant enzyme into an ATP regeneration system containing 10 μM NADH plus 100 and 200 nM ATP, respectively. Trace e was obtained after injecting the double-mutant enzyme into the regeneration system containing 20 μM NADH plus 400 nM ATP. The numbers at the ends of traces c−e represent the rates of NADH consumption in μmol oxidized min^{-1} (mg of enzyme)$^{-1}$ that were calculated from the slopes of the traces recorded between 10 and 15 min after adding the enzyme. Table 2 compares the observed rates of ATP hydrolysis indicated on traces c−e of Figure 5, with the rate calculated from the Michaelis−Menten equation using a V_{max} of 37 μmol of ATP hydrolyzed mg^{-1} min^{-1} and a K_m of 31 μM obtained from Figure 4. The experimental rates in Table 2 were corrected for the rates of NADH

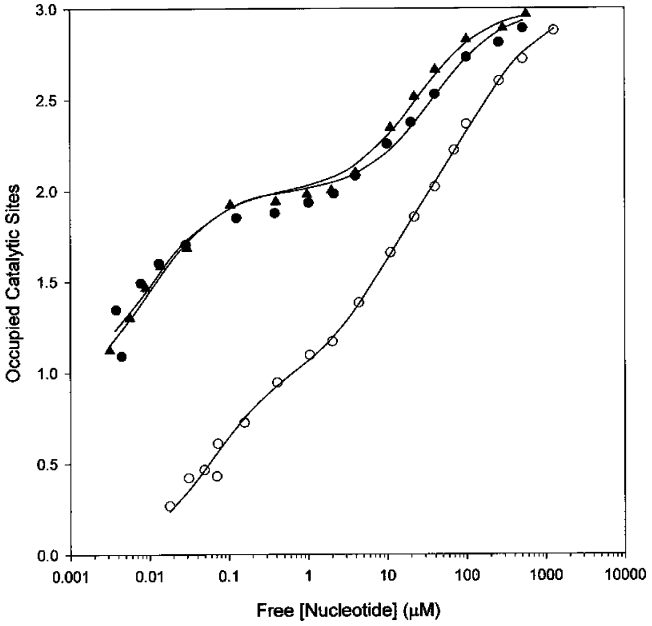

FIGURE 6: Fluorescence titrations of the introduced tryptophans in the $\alpha_3(\beta M^{222}S/Y^{345}W)_3\gamma$ double-mutant subcomplex with MgADP, MgATP, and ATP. The fluorescence titrations were performed as described in the Experimental Procedures. (▲) Titration with MgADP, (●) titration with MgATP, and (○) titration with ATP.

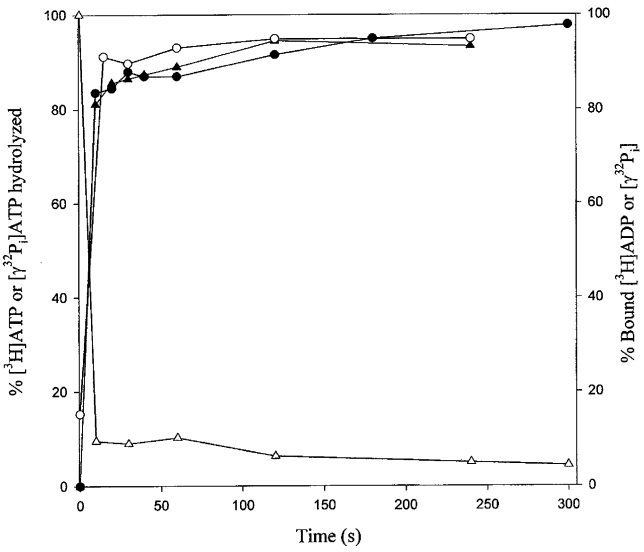

FIGURE 7: Hydrolysis of substoichiometric [^{3}H]ATP and [^{32}P]ATP by the wild-type $\alpha_3\beta_3\gamma$ subcomplex. The extent of hydrolysis of 1.7 μM [^{3}H]ATP and 1.7 μM [γ-^{32}P]ATP by 2.85 μM wild-type subcomplex was determines as described in the Experimental Procedures. (●) Percent of [^{3}H]ATP hydrolyzed, (▲) percent of [γ-^{32}P]ATP hydrolyzed, (○) percent of [^{3}H]ADP remaining bound, and (△) percent of [^{32}P$_i$] remaining bound.

consumption observed when the enzyme was added to the regeneration system in the absence of added ATP. The calculated and experimentally determined rates are similar. Therefore, it is reasonable to conclude that the $\beta M^{222}S/Y^{345}W$ double-mutant enzyme hydrolyzes 200 nM ATP with a rate of about 0.25 μmol mg^{-1} min^{-1}, which corresponds to a k_{cat} of 1.5 s^{-1}.

Comparison of the Affinities of Catalytic Sites in the $\beta M^{222}S/Y^{345}W$ Double Mutant for Nucleotides Obtained from Fluorescence Titrations of the Introduced Tryptophans. Figure 6 illustrates titrations of the introduced tryptophans in the $\beta M^{222}S/Y^{345}W$ double mutant with MgADP, MgATP, and ATP in the absence of the Mg^{2+} ion. In each titration, the three catalytic sites in the double-mutant enzyme exhibited different affinities for the nucleotide. After the addition of stoichiometric MgADP or MgATP to the double-mutant enzyme, one-third of the fluorescence was quenched. Therefore, in titrations with MgADP and MgATP, K_{d_1}, the binding constant for the catalytic site of the highest affinity, was too low to be determined by this method. In contrast, a K_{d_1} value of 50 nM was obtained from the titration of the double-mutant subcomplex with free ATP. The K_{d_2} values obtained from titrations with MgADP and MgATP are 12 and 11 nM, respectively. The apparent K_{d_2} value obtained from the titration with ATP in the absence of $MgCl_2$ is 8 μM. The K_{d_3} values obtained from titrations with MgADP and MgATP are 25 and 37 μM, respectively. The apparent K_{d_3} value obtained from the titration with free ATP is 160 μM.

Hydrolysis of Substoichiometric ATP by the Wild-Type $\alpha_3\beta_3\gamma$ Subcomplex. As described here for the $\beta M^{222}S/Y^{345}W$ double mutant, Dou et al. (*23*) found that the addition of stoichiometric MgATP to the $\beta Y^{345}W$ single mutant decreased fluorescence emission by 33% within 30 s. Fluorescence quenching remained at 33% after 60 min. The $\alpha_3(\beta M^{222}S/Y^{345}W)_3\gamma$ double-mutant subcomplex behaves in the same manner in that quenching of the tryptophan fluorescence remained at about 33% 10 min after mixing it with stoichiometric MgATP.

These observations are inconsistent with the characteristics of hydrolysis of substoichiometric [α,γ-^{32}P]ATP by five subunit TF_1 ($\alpha_3\beta_3\gamma\delta\epsilon$) reported by Yohda and Yoshida (*24*). They reported that substoichiometric [α,γ-^{32}P]ATP was completely hydrolyzed within 5 min after mixing it with the five-subunit enzyme. Hydrolysis was accompanied by rapid release of both [α-^{32}P]ADP and $^{32}P_i$. It is possible that retention of nucleotides on the high-affinity catalytic site observed in fluorescence titrations of mutant subcomplexes containing the $\beta Y^{345}W$ substitution might be caused by the interaction of the side chain of the introduced tryptophan with the adenine of the bound nucleotide. To test this possibility, hydrolysis of substoichiometric [^{3}H]ATP and [γ-^{32}P]ATP by the wild-type $\alpha_3\beta_3\gamma$ subcomplex of TF_1 was examined.

Figure 7 illustrates hydrolysis of substoichiometric [^{3}H]ATP and substoichiometric [γ-^{32}P]ATP by the wild-type $\alpha_3\beta_3\gamma$ subcomplex and the amounts of [^{3}H]ADP or $^{32}P_i$ remaining bound to the enzyme following hydrolysis. About 90% of the added [^{3}H]ATP or [γ-^{32}P]ATP was hydrolyzed within 2 min. After hydrolysis of [^{3}H]ATP, all of the product [^{3}H]ADP remained bound to the enzyme. In contrast, at least 90% of product $^{32}P_i$ was released rapidly when the wild-type subcomplex hydrolyzed [γ-^{32}P]ATP. In experiments not illustrated, it was also shown that the $\beta M^{222}S/^{345}W$ double-mutant enzyme hydrolyzes at least 90% of the substoichiometric [^{3}H]ATP added to it within 2 min that was accompanied with the complete retention of the product [^{3}H]ADP. It is clear that the wild-type and $\alpha_3(\beta M^{222}S/Y^{345}W)_3\gamma$ double-mutant subcomplexes hydrolyze substoichiometric ATP with different characteristics than those reported for the $\alpha_3\beta_3\gamma\delta\epsilon$ TF_1 complex (*24*).

DISCUSSION

The K_m value of 31 μM obtained from steady-state kinetic analysis of the $\beta M^{222}S/Y^{345}W$ double-mutant enzyme is similar to the K_{d_3} value of 37 μM obtained from fluorescence titration of its introduced tryptophans with MgATP. The K_{d_2} value obtained from the fluorescence titration of the double mutant with MgATP is about 12 nM. Because the double-mutant enzyme hydrolyzes 200 nM ATP with a first-order rate of 1.5 s^{-1}, it is clear that it does not hydrolyze ATP at a significant rate until the catalytic site of the lowest affinity binds MgATP. This contradicts the conclusion recently reported by Milgom and Cross (*19*) that, after incubation with magnesium pyrophosphate (Mg-PP_i), bovine MF_1 depleted of endogenous nucleotides ($ndMF_1$) attains maximal velocity when the catalytic site of the intermediate affinity is saturated with MgATP. Saturation of noncatalytic sites with Mg-PP_i prevents entrapment of inhibitory MgADP in a catalytic site during ATP hydrolysis catalyzed by $ndMF_1$ (*7*).

To account for the different catalytic characteristics of $ndMF_1$ reported by Milgrom and Cross (*19*) and those of the $\beta M^{222}S/Y^{345}W$ double-mutant enzyme reported here, it might be argued that the two amino acid substitutions at or near the catalytic site in the double-mutant subcomplex convert the enzyme from a bi- to a trisite mechanism for ATP hydrolysis. However, the following observations suggest that the wild-type TF_1 subcomplex also attains maximal velocity upon saturation of the catalytic site of the lowest affinity. (1) In the presence or absence of LDAO, the wild-type subcomplex hydrolyzes 2 μM−2 mM ATP with a K_m of 43 μM (*16*, *17*). (2) After incubation with 50 μM [^{3}H]ADP and 2 mM $MgCl_2$, the wild-type TF_1 subcomplex retains 1.9 mol of [^{3}H]ADP/mol after passage through a Sephadex G50 centrifuge column (*25*, *26*). This indicates that the K_{d_2} value of the wild-type subcomplex for MgADP is considerably lower than 43 μM.

On the other hand, the catalytic characteristics and affinities of the catalytic sites for nucleotides of the $ndMF_1$ preparation examined by Milgrom and Cross (*19*) differ considerably from those described in other reports (*7*, *15*, *27*, *28*). Their $ndMF_1$ preparation displayed K_m and k_{cat} values of about 77 μM and 370 s^{-1}, respectively, at 22 °C, and displayed a k_{cat} value of about 765 s^{-1} at 30 °C. In contrast, Kalashnikova et al. (*27*) reported that $ndMF_1$ exhibits K_m and k_{cat} values of 125 μM and 765 s^{-1}, respectively, at 25 °C, and Milgrom et al. (*15*) reported that $ndMF_1$ exhibits K_m and k_{cat} values of 133 μM and 700 s^{-1}, respectively, at 25 °C. Furthermore, Jault and Allison reported that $ndMF_1$ hydrolyzes ATP at 30 °C with K_m and k_{cat} values of 120 μM and 1350 s^{-1}, respectively (*7*). Therefore, the $ndMF_1$ preparation described in ref *19* hydrolyzed ATP with k_{cat} values that are about 50% of those described by others (*7*, *15*, *27*) and had an unusually low K_m value, suggesting that it had defective catalytic properties.

We also have reservations about the method described in ref *19* to estimate the K_{d_1} and K_{d_2} values for ATP binding to catalytic sites of $ndMF_1$. Bound [^{3}H]ANP was estimated by transferring 400 μL volumes of reaction mixtures containing 0.85 μM $ndMF_1$ and various concentrations of [^{3}H]ATP in an ATP regeneration system to the sample reservoir of membrane filter devices that were then submitted to two short intervals of centrifugation. Because the membrane filters were preserved in glycerol, the first filtrate was discarded. The amount of [^{3}H]ANP in the second filtrate was used to calculate the amount of [^{3}H]ANP remaining bound to MF_1. A K_{d_1} value of 15 nM and a K_{d_2} value of 78 μM were obtained from a semilogarithmic plot of bound [^{3}H]ANP against the free [^{3}H]ATP concentration obtained from the membrane filtration assays. In contrast, the K_{d_1} value of 15 nM obtained from membrane filtration analysis is inconsistent with an earlier report that estimated the association constant of ATP binding to the high-affinity catalytic site of MF_1 to be about 10^{12} M^{-1} (*29*). The glycerol present in the membrane filtration device used by Milgrom and Cross to estimate K_d values might be responsible for the large discrepancy between the K_{d_1} value that they reported and the association constant reported for MF_1 by Grubmeyer et al. (*29*).

The finding that the wild-type $\alpha_3\beta_3\gamma$ subcomplex hydrolyzes substoichiometric MgATP with the retention of ADP and rapid release of P_i is consistent with the results of stopped-flow analysis of hydrolysis of substoichiometric MgATP by the $\alpha_3(\beta R^{337}W)_3\gamma$ mutant subcomplex of TF_1 reported by Masaike et al. (*30*). The $\beta R^{337}W$ mutant hydrolyzes substoichiometric MgATP with a k_{cat} of 14 s^{-1}. After hydrolysis, ADP was retained, whereas P_i was released with a rate constant of 2.8 s^{-1}. Therefore, the wild-type and $\beta R^{337}W$ mutant subcomplexes do not hydrolyze substoichiometric MgATP with an equilibrium constant near unity. In contrast, it has been reported that MF_1, with and without endogenous nucleotides (*28*, *29*), and EF_1 containing endogenous nucleotides (*31*) hydrolyze substoichiometric ATP with equilibrium constants near unity.

This study was initiated when it was found that the $\alpha_3(\beta M^{222}S)_3\gamma$ single-mutant subcomplex has low propensity to entrap inhibitory MgADP in a catalytic site during turnover. It hydrolyzes 50 μM ATP with a nearly linear initial rate. In contrast, the $\beta M^{222}S/Y^{345}W$ double-mutant enzyme hydrolyzes low concentrations of ATP with an accelerating initial rate unless it was incubated with at least 30 μM ATP before initiating assays with Mg^{2+} ion. Linear initial rates were also observed after incubating 1.43 μM double-mutant enzyme with between a 3.5−7.0-fold molar excess of MgADP before initiating assays. These observations suggest that the accelerating rates observed when the double-mutant enzyme hydrolyzes ATP, in the absence of prior incubation of nucleotides, represent a slow conformational change that occurs after loading catalytic sites with nucleotides or slow binding of nucleotides to noncatalytic sites. Slow binding of MgATP to catalytic sites is not responsible for the accelerating rates observed in the absence of prior incubation of the double-mutant enzyme with nucleotides for the following reason. Maximal quenching of the tryptophan fluorescence occurred within 30 s of mixing MgATP with the double-mutant subcomplex at all concentrations examined. In contrast, the lag observed during hydrolysis of 50 μM ATP by the double-mutant enzyme illustrated in Figure 1, lasted several minutes.

Two observations are consistent with the premise that the accelerating initial rates observed represent a slow conformational change that occurs after loading two catalytic sites with nucleotides. (1) Rates of hydrolysis of each concentration of ATP (20 μM−2 mM) used in the Lineweaver−Burk

plot illustrated in Figure 4 became linear in about 5 min. This suggests that the accelerating initial rates are not caused by the slow binding of MgATP to noncatalytic sites but rather to a slow conformational change after loading catalytic sites. (2) The fluorescence titration of the double-mutant enzyme with ATP in the absence of the Mg^{2+} ion illustrated in Figure 6 shows that the catalytic site of the intermediate affinity saturates in the presence of 30−40 μM ATP. This is consistent with the observation that linear initial rates of ATP hydrolysis were not observed unless the double-mutant enzyme was incubated with at least 30 μM ATP before initiating assays with $MgCl_2$. However, inconsistent with these observations, Figure 3B shows that an accelerating initial rate was observed after incubating 1.43 μM double-mutant enzyme (0.5 mg/mL) with a 3.5 molar excess of MgADP before injecting a 1 μg sample into 1 mL of the assay medium containing 50 μM MgATP. It is possible that this discrepancy might have been caused by the 500-fold dilution that occurred when the pretreated enzyme was injected into the assay medium to determine the initial rate of ATP hydrolysis. In any case, the catalytic site of the lowest affinity must be occupied to observe significant rates of ATP hydrolysis.

As pointed out by Wilke-Mounts et al. (*32*), βMet^{222} is conserved in all F_1-ATPases that have been sequenced and its side chain is near side chains of βGlu^{188} and βArg^{260} in crystal structures of MF_1. The carboxyl group of βE^{188} functions as a general base that deprotonates the attacking water molecule during ATP hydrolysis (*1*, *2*). Ahmad and Senior (*33*) have shown that substitution of βR^{260} with Gln, Lys, or Ala impairs ATP synthesis catalyzed by *E. coli* membrane vesicles. Furthermore, EF_1 preparations containing each of these amino acid substitutions do not form inhibitory MgADP−fluoroaluminate or MgADP−fluoroscandinate complexes in catalytic sites and exhibit severely reduced rates of ATP hydrolysis. As pointed out by Ahmad and Senior (*33*), these observations suggest that the guanidinium of βR^{260} participates in binding P_i to the empty catalytic site of F_1 during ATP synthesis. Wilke-Mounts et al. (*32*) showed that membrane vesicles containing EF_1 with the βM^{222}V, βM^{222}L, βM^{222}I, and βM^{222}F substitutions have essentially no ATPase activity, whereas membrane vesicles containing EF_1 with the βMet^{222}Gln substitution have substantial ATPase activity. These observations suggest that the lone electron pair on the sulfur atom in the side chain of βM^{222} in wild-type F_1-ATPases might influence the positions of βE^{188} and/or βR^{260} in a productive manner during ATP hydrolysis.

It is not clear how amino acid substitutions at or near catalytic sites in the $\alpha_3\beta_3\gamma$ subcomplex of TF_1 affect entrapment of inhibitory MgADP during turnover. As originally shown in yeast MF_1 (*34*, *35*), the $\alpha_3\beta_3\gamma$ subcomplex of TF_1 containing the βT^{163}S substitution has a very low propensity to entrap inhibitory MgADP in a catalytic site during turnover (*36*). In crystal structures of MF_1 (*2*−*5*), the oxygen in the side chain of βThr^{163} is directly liganded to Mg^{2+} ions complexed with nucleotides at catalytic sites. However, in unpublished experiments, we showed that the βT^{163}S/Y^{345}W double-mutant subcomplex hydrolyzes ATP with nearly the same characteristics exhibited by the βY^{345}W single-mutant subcomplex. The βY^{345}W single-mutant and βT^{163}S/Y^{345}W double-mutant subcomplexes hydrolyze 50 μM ATP with a fast initial rate that rapidly decelerates into a slower rate. Deceleration is caused by turnover-dependent entrapment of inhibitory MgADP in a catalytic site.

In the *N*,*N*′-dicyclohexylcarbodiimide (DCCD)-MF_1 and ADP-MF_1 crystal structures (*4*, *5*), the guanidinium of αArg^{373} is hydrogen-bonded to the 2′-hydroxyl of ADP bound to the catalytic site at the α_{TP}/β_{TP} interface. As pointed out earlier (*37*), this probably represents the structure of a catalytic site containing inhibitory MgADP. It is possible that amino acid substitutions in F_1-ATPases that reduce or eliminate entrapment of inhibitory MgADP in a catalytic site during turnover induce global effects that prevent the guanidinium of αR^{376} from forming an abortive interaction with the 2′-hydroxyl of ADP bound to a catalytic site.

REFERENCES

1. Yoshida, M., Muneyuki, E., and Hisabori, T. (2001) ATP synthase−A marvelous rotary engine of the cell, *Nat. Rev. Mol. Cell Biol. 2*, 669−677.
2. Abrahams, J. P., Leslie, A. G. W., Lutter, R., and Walker, J. E. (1994) Structure at 2.8 Å resolution of F_1-ATPase from bovine heart mitochondria, *Nature 370*, 621−628.
3. Menz, R. I., Walker, J. E., and Leslie, A. G. W. (2001) Structure of bovine mitochondrial F_1-ATPase with nucleotide bound to all three catalytic sites: Implications for mechanism of rotary catalysis, *Cell 106*, 331−341.
4. Gibbons, C., Montgomery, M. G., Leslie, A. G. W., and Walker, J. E. (2000) The structure of the central stalk in bovine F_1-ATPase at 2.4 Å resolution, *Nat. Struct. Biol. 7*, 1055−1061.
5. Kagawa, R., Montgomery, M. G., Braig, K., Leslie, A. G. W., and Walker, J. E. (2004) The structure of bovine F_1-ATPase inhibited by ADP and beryllium fluoride, *EMBO J. 23*, 2734−2744.
6. Ren, H., and Allison, W. S. (2000) On what makes the γ subunit spin during ATP hydrolysis by F_1, *Biochim. Biophys Acta 1458*, 221−233.
7. Jault, J.-M.; Allison, W. S. (1993) Slow binding of ATP to noncatalytic nucleotide binding sites which accelerates catalysis is responsible for apparent negative cooperativity exhibited by the bovine mitochondrial F_1-ATPase, *J. Biol. Chem. 268*, 1558−1566.
8. Jault, J.-M., Matsui, T., Jault, F. M., Kaibara, C., Muneyuki, E., Yoshida, M., Kagawa, Y., and Allison, W. S. (1996) The $\alpha_3\beta_3\gamma$ complex of the F_1-ATPase from thermophilic *Bacillus* PS3 containing the αD^{261}N substitution fails to dissociate inhibitory MgADP from a catalytic site when ATP binds to noncatalytic sites, *Biochemistry 34*, 16412−16418.
9. Noji, H., Yasuda, R., Yoshida, M., and Kinosita, K. (1997) direct observation of the rotation of F_1-ATPase, *Nature 386*, 299−302.
10. Yasuda, R., Noji, H., Yoshida, M., Kiosita, K., and Itoh, H. (2001) Resolution of distinct rotational substeps by millisecond kinetic analysis of F_1-ATPase, *Nature 410*, 898−904.
11. Boyer, P. D. (1989) A perspective of the binding change mechanism for ATP synthesis, *FASEB J. 3*, 2164−2178.
12. Cross, R. L., Grubmeyer, C., and Penefsky, H. S. (1982) Mechanism of ATP hydrolysis by beef heart mitochondrial ATPase, *J. Biol. Chem. 257*, 12101−12105.
13. Duncan, T. M., and Senior, A. E. (1985) The defective proton-ATPase of uncD mutants of *Escherichia coli*: Two mutations which affect the catalytic mechanism, *J. Biol. Chem. 260*, 4901−4907.
14. Weber, J., Wilke-Mounts, S., Lee, R. S., Grell, E., and Senior, A. E. (1993) Specific placement of tryptophan in the catalytic sites of *Escherichia coli* F_1-ATPase provides a direct probe of nucleotide binding: Maximal ATP hydrolysis occurs with three sites occupied, *J. Biol. Chem. 268*, 20126−20133.
15. Milgrom, Y. M., Murataliev, M. B., and Boyer, P. D. (1998) Bi-site activation occurs with native and nucleotide-depleted mitochondrial F_1-ATPase, *Biochem. J. 330*, 1037−1043.
16. Ren, H. M., and Allison, W. S. (2000) Substitution of βGlu^{201} in the $\alpha_3\beta_3\gamma$ subcomplex of the F_1-ATPase from the thermophilic *Bacillus* PS3 increases the affinity of catalytic sites for nucleotides, *J. Biol. Chem. 275*, 10057−10063.
17. Bandyopadhyay, S., Valder, C. R., Huynh, H. G., Ren, H., and Allison, W. S. (2002) The βG^{156}C substitution in the F_1-ATPase

from the thermophilic *Bacillus* PS3 affects catalytic cooperativity by destabilizing the closed conformation of the catalytic site, *Biochemistry 41*, 14421−14429.
18. Ono, S., Hara, S. K., Hirao, J., Matsui, H., Noji, H., Yoshida, M., and Muneyuki, E. (2003) Origin of apparent negative cooperativity of F_1-ATPase, *Biochim. Biophys. Acta 1607*, 35−44.
19. Milgrom, Y. M., and Cross, R. L. (2005) Rapid hydrolysis of ATP by mitochondrial F_1-ATPase correlates with filling of the second of three catalytic sites, *Proc. Natl. Acad. Sci. U.S.A. 102*, 13831−13836.
20. Matsui, T., and Yoshida, M. (1995) Expression of wild-type and the Cys-/Trp-less $\alpha_3\beta_3\gamma$ complex of thermophilic F_1-ATPase in *Escherichia coli*, *Biochim. Biophys. Acta 1231*, 139−146.
21. Penefsky, H. S. (1977) Reversible binding of P_i by beef heart mitochondrial adenosine triphosphatase, *J. Biol. Chem 252*, 2891−2899.
22. Bradford, M. M. (1976) A rapid and sensitive method for the quantitation of microgram quantities of protein utilizing the principle of protein−dye binding, *Anal. Biochem. 72*, 248−254.
23. Dou, C., Fortes, P. A. G., and Allison, W. S. (1998) The $\alpha_3(\beta Y^{341}W)_3\gamma$ subcomplex of the F_1-ATPase from the thermophilic *Bacillus* PS3 fails to dissociate ADP when MgATP is hydrolyzed at a single catalytic site and attains maximal velocity when three catalytic sites are saturated, *Biochemistry 37*, 16757−16764.
24. Yohda, M., and Yoshida, M. (1987) Single site catalysis of F_1-ATPase from thermophilic bacterium PS3 and its dominance in steady-state catalysis at low ATP concentration, *J. Biochem. 102*, 875−883.
25. Dou, C., Grodsky, N. B., Matsui, T., Yoshida, M., and Allison, W. S. (1997) ADP−fluoroaluminate complexes are formed cooperatively at two catalytic sites of the wild-type and mutant $\alpha_3\beta_3\gamma$ subcomplexes of the F_1-ATPase from the thermophilic *Bacillus* PS3, *Biochemistry 36*, 3719−3727.
26. Grodsky, N. B., Dou, C., and Allison, W. S. (1998) Mutations in the nucleotide binding domain of the α subunits of the F_1-ATPase from the thermophilic *Bacillus* PS3 that affect cross-talk between nucleotide binding sites, *Biochemistry 37*, 1007−1014.
27. Kalashnikova, T. Y., Milgrom, Y. M., and Murataliev, M. B. (1988) The effect of inorganic pyrophosphate on the activity and P_i-binding properties of mitochondrial F_1-ATPase, *Eur. J. Biochem. 177*, 213−218.
28. Milgrom, Y. M., and Cross, R. L. (1997) Nucleotide-depleted beef heart F_1-ATPase exhibits strong positive cooperativity, *J. Biol. Chem. 272*, 32211−32214.
29. Grubmeyer, C., Cross, R. L., and Penefsky, H. S. (1982) Mechanism of ATP hydrolysis by beef heart mitochondrial ATPase. Rate constants for elementary steps in catalysis at a single site, *J. Biol. Chem. 257*, 12092−12100.
30. Masaike, T., Muneyuki, E., Noji, H., Kinosita, K., Jr., and Yoshida, M. (2002) F_1-ATPase changes its conformation upon phosphate release, *J. Biol. Chem. 277*, 21643−21649.
31. Al-Shawi, M. K., and Senior, A. E. (1988) Complete kinetic and thermodynamic characterization of the unisite catalytic pathway of *Escherichia coli* F_1-ATPase, *J. Biol. Chem. 263*, 19640−19648.
32. Wilke-Mounts, S., Pagan, J., and Senior, A. E. (1995) Mutagenesis and reversion analysis of residue Met-209 of the β-subunit of *Escherichia coli* ATP synthase, *Arch. Biochem. Biophys. 324*, 153−158.
33. Ahmad, Z., and Senior, A. E. (2004) Mutagenesis of residue βArg-246 in the phosphate-binding subdomain of catalytic sites of *Escherichia coli* F_1-ATPase, *J. Biol. Chem 279*, 31505−31513.
34. Mueller, D. M. (1989) A mutation altering the kinetic responses of yeast mitochondrial F_1-ATPase, *J. Biol. Chem. 264*, 16552−16556.
35. Mueller, D. M., Indyk, V., and McGill, L. (1994) ATPase kinetics for wild-type *Saccharomyces cerevisiae* F_1-ATPase and F_1-ATPase with the β-subunit Thr^{197}-Ser mutation, *Eur. J. Biochem. 222*, 991−999.
36. Jault, J.-M., Dou, C., Grodsky, N. B., Matsui, T., Yoshida, M., and Allison, W. S. (1996) The $\alpha_3\beta_3\gamma$ subcomplex of the F_1-ATPase from the thermophilic *Bacillus* PS3 with the $\beta T^{165}S$ substitution does not entrap inhibitory MgADP in a catalytic site during turnover, *J. Biol. Chem. 271*, 28818−28824.
37. Bandyopadhyay, S., Muneyuki, E., and Allison, W. S. (2005) The characteristics of the $(\alpha V^{371}C)_3(\beta R^{337}C)_3\gamma$ double mutant of the TF_1-ATPase indicate that the catalytic site at the $\alpha_{TP}-\beta_{TP}$ interface with bound MgADP in crystal structures of MF_1 represents a catalytic site containing inhibitory MgADP, *Biochemistry 44*, 2441−2448.

BI060232W